Benchmarking an even better top tagger algorithm

Christoph Anders,[1] Catherine Bernaciak,[2] Gregor Kasieczka,[3] Tilman Plehn,[2] and Torben Schell[2]

[1]*Physikalisches Institut, Universität Heidelberg, 69120 Heidelberg, Germany*
[2]*Institut für Theoretische Physik, Universität Heidelberg, 69120 Heidelberg, Germany*
[3]*Institute for Particle Physics, ETH Zürich, 8093 Zürich, Switzerland*

Top taggers are established analysis tools used to reconstruct boosted hadronically decaying top quarks, for example, in searches for heavy resonances. We first present a dedicated study of signal efficiency versus background rejection, allowing for an improved choice of working points. Next, we determine to what degree our mass drop selection can be improved by systematically including angular correlations between subjets or N-subjettiness. Finally, we extend the reach of the top tagger to transverse momenta below the top mass. This momentum range will be crucial in searches for the associated production of a Higgs boson with top quarks.

I. INTRODUCTION

Because the top quark is the only observed fermion with a weak-scale mass, it can be expected to have strong ties with the mechanism of electroweak symmetry breaking. Models which attempt to solve the hierarchy problem, like supersymmetry, top color, or little Higgs models [1], predict additional states in the top sector to ameliorate the effect of the top quark on the Higgs boson's mass. In the Higgs sector we can test modifications of the top Yukawa coupling in the associated production of a Higgs boson with a top pair [2–4]. An example for weakly interacting physics beyond the Standard Model, which modifies the top Yukawa coupling and can be used to complete the Standard Model with free Higgs couplings in the ultraviolet, is a two Higgs doublet model [5]. Typical signatures of new physics linked to the top sector include top partners decaying to top quarks and missing energy [6–8], heavy resonances decaying to two boosted tops [9,10], or single top production [11].

The ultimate experimental goal at the LHC is to search for such effects in different decay channels, including the purely hadronic decay of two top quarks. In purely hadronic analyses we first have to overcome the multijet QCD background [12]. After that initial step we have to extract the signal out of top pair backgrounds, using the kinematics of the reconstructed tops. Recently, we have seen that the most promising phase space region for both of these tasks is that of boosted top decays with $p_{T,t} \gtrsim m_t$ [13]. Such a boost will, aside from other improvements, separate the decay products of two top quarks and offer a handle against combinatorial backgrounds [2,12].

While hadronic signatures are the target of top taggers, experimental tests have to be performed with an event sample that can be easily controlled. Semileptonic top pairs can be triggered based on a hard lepton. The momentum of the lepton will also be strongly correlated with the transverse momentum of the hadronically decaying top quark. If necessary, b tags can be used to control $W +$ jets backgrounds. Because the aim of this paper is to improve the top tagging efficiency, in particular, towards lower transverse momenta, we will present all of our findings in terms of semileptonic top pairs, so they can be easily reproduced by ATLAS and CMS.

The idea of studying the substructure of jets and using this structure to identify massive hadronically decaying particles has been around for almost 20 years [9,14,15]. In the following we will focus on tagging top quarks [2,7,16–21] with the help of the HEPTOPTAGGER and in a moderately boosted regime with $p_{T,t} \lesssim 800$ GeV. In this framework ATLAS has published promising results [22], motivating this detailed study of top tagging in the upcoming 13 TeV run. To identify and reconstruct hadronic top decays with higher boost, there exist specific HEPTOPTAGGER improvements [23]. Our study will be based on semileptonic top pair events, which allows for relatively easy experimental tests in data.

As a first step we will introduce some minor modifications of the HEPTOPTAGGER algorithm in Sec. II. We will mostly target a possible shaping of QCD backgrounds towards an unphysical peak in the reconstructed top mass at low and high jet multiplicities. For this new default setup we will, for the first time, introduce receiver operating characteristics (ROC) curves to quantify the performance of the tagger beyond the known working points. In Sec. III we will extend the available observables in the tagging procedure by angular correlations, given in terms of Fox-Wolfram moments [24,25]. In Sec. IV we will, in a similar spirit, test the combination of the HEPTOPTAGGER with N-subjettiness. Finally, in Sec. V we will modify the tagging algorithm such that we can identify and reconstruct boosted tops down to $p_{T,t} = 150$ GeV, as suggested by the MADMAX study of the $t\bar{t}H$ process [26].

II. THE NEW DEFAULT

In this first section we test two modifications of the HEPTOPTAGGER algorithm [7]. None of them will significantly change the performance of the tagger in terms of signal efficiency and background rejection. However, they are relevant for the reconstructed m_t^{rec} distribution for the QCD multijet background. Our signal event sample contains semileptonic decays ($\ell = e, \mu$) of $t\bar{t}$ pairs with up to two additional matrix element jets, generated with ALPGEN [27] and PYTHIA [28] using MLM merging [29]. For the background we consider a leptonically decaying W plus two to four matrix element jets simulated the same way. On the generator level all hard jets have to fulfill $p_{T,j} > 25$ GeV, $|\eta_j| < 5$, and $\Delta R_{jj} > 0.4$. The top mass used for simulation is 173 GeV. We initially study the current collider energy of $\sqrt{s} = 8$ TeV and will then move to $\sqrt{s} = 13$ TeV.

Throughout our analysis the top tagging algorithm operates on fat jets with the Cambridge-Aachen size $R_{\text{fat}} = 1.8$, reconstructed by FASTJET [30,31]. In this section we require fat jets with $p_{T,\text{fat}} > 200$ GeV and $|\eta_{\text{fat}}| < 2.5$. The increased size as compared to the old default of $R_{\text{fat}} = 1.5$ will allow us to increase the tagging efficiency for moderate boost. This increase is triggered by the encouraging experimental studies of pile-up in filtered fat jets [32], but it might lead to a readjustment of the filtering parameters. For consistency we only accept tagged tops with $p_{T,\text{tag}} > 200$ GeV in this first step. We give all other tagging parameters in Table I: The mass drop required for a massive splitting is defined by min $m_{j_{1,2}}/m_j < f_{\text{drop}} = 0.8$. The jet algorithm stops at subjets with $m_{\min} = 30$ GeV, where this parameter can be easily adapted to a more challenging detector environment. The W and top masses are defined on a filtered set of subjets allowing for $N_{\text{filt}} = 5$ objects, i.e. including up to two jets from final state radiation. The kinematic conditions are parametrized by the HEPTOPTAGGER variables $R_{\text{min,max}} = (0.85 - 1.15) \times m_W/m_t$, arctan $m_{13}/m_{12} = 0.2 - 1.3$, and $m_{23}/m_{123} > 0.35$. The selected region has an A-like shape in the two-dimensional plane [7]. Finally, the mass window of the reconstructed top mass is 150–200 GeV, while in the old default setup we do not apply a specific cut on the ratio of the reconstructed W and top masses.

Our first modification of the HEPTOPTAGGER algorithm affects the order in which we apply the top mass selection and the A-shaped W mass constraints. In the standard algorithm, early on we select a filtered triplet of hard subjets closest to the top mass [7]. This triplet is then required to fulfill the different W and top mass cuts. The danger is that in the presence of more than one valid triplet of filtered subjets, we pick the wrong one such that we are guaranteed not to pass the W mass constraints. To avoid this, we can first preselect all triplets which pass the mass cuts and then pick the one with m_{123} closest to m_t out of those passing the W mass constraints. In Fig. 1 we first see that both versions work on the signal events without an appreciable difference. The standard ordering slightly shapes the background around $m_t \sim m_{123}$.

The tagging efficiency and mistagging rates for both approaches applied to semileptonic top pairs are given in Table II. The signal efficiencies are defined as the number of tagged tops divided by the number of hadronically decaying tops in the event sample with $p_{T,t} > 200$ GeV and $|\eta_t| < 2.5$. For the background we quote the number of mistags in the leptonic $W + $ jets sample per number of fat jets passing $p_{T,\text{fat}} > 200$ GeV and $|\eta_{\text{fat}}| < 2.5$. We see that with the new ordering both the signal efficiency and the background mistagging rate increase, such that typical significances stay constant. Based on the reduced shaping of the background mass distributions we will assume the new order of cuts as HEPTOPTAGGER standard.

If the algorithm described above is used in a high-multiplicity environment, caused by multijet final states and contributions from pileup, it is not guaranteed that there is a unique triplet of filtered subjets which corresponds to the three top decay partons. The same problem arises for the Higgs tagger in the semileptonic boosted $t\bar{t}H$ analysis. In that situation choosing the combination with $|m_{12} - m_H|$, or in this case $|m_{123} - m_t|$, is guaranteed to shape the background. To construct an alternative criterion for choosing the correct combination of subjets, we start with the observation that the jet mass can be approximately linked to the Jade distance [33],

$$m_{ij}^2 \simeq E_i E_j \Omega_{ij}^2 \simeq p_{T,i} p_{T,j} (\Delta R_{ij})^2. \tag{1}$$

We can reweight the transverse momenta and the geometric separation to construct an alternative metric for choosing subjet combinations, like, for example, the modified Jade distance summed over the three top decay subjet candidates,

$$dj_{\text{sum}} = \sum_{(ij)} d_{ij} \qquad \text{with } d_{ij} = p_{T,i} p_{T,j} (\Delta R_{ij})^4. \tag{2}$$

TABLE I.   Parameters in the HEPTOPTAGGER algorithm, as defined in the text.

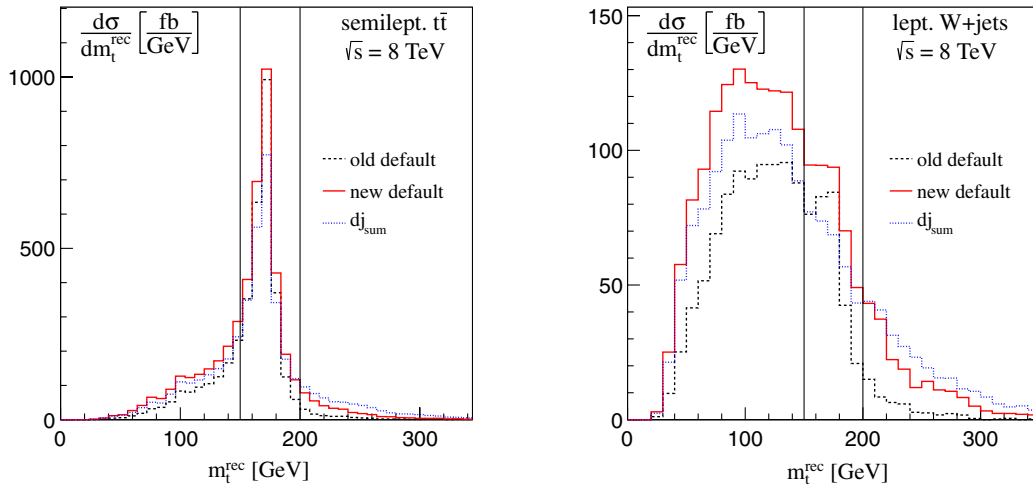| R_{fat}	1.8	$R_{\text{min,max}}$	$(0.85 - 1.15) \times m_W/m_t$
f_{drop}	0.8	m_{23}/m_{123} and arctan m_{13}/m_{12} cuts	0.35, 0.2, 1.3
$m_{\min}$ [GeV]	30	m_t^{rec} [GeV]	150–200
N_{filt}	5	$(m_W/m_t)^{\text{rec}}/(m_W/m_t)$	no cut

FIG. 1 (color online).   Reconstructed top mass for the signal (left panel) and background (right panel) samples at 8 TeV collider energy. We show the standard order of cuts with $|m_{123} - m_t|$ selection (dashed black line), the inverted order of cuts with $|m_{123} - m_t|$ selection (solid red line), and the inverted order of cuts with dj_{sum} selection (dotted blue line).

When we ask for the maximum modified Jade distance, we enhance the weight of the geometric separation as compared to the jet mass; i.e. we prefer those subjet combinations which are more widely separated. In Fig. 1 we compare the m_t^{rec} distributions with the old and new HEPTopTagger default setups. For the signal as well as the background sample, we find less candidates in the mass window 150–200 GeV. In addition, the background is even less shaped than for the inverted ordering described above. The corresponding (mis)tagging efficiencies are given in Table II. While we find a tiny improvement in the signal-to-background ratio compared to the new default setup, the signal efficiency is significantly reduced. We therefore include this new selection according to Eq. (2) as an option for high-multiplicity applications of the HEPTopTagger, but we do not make it the new default setting.

To conclusively test the performance of any algorithm, like the HEPTopTagger, it is not sufficient to only study a single operating point like the one described in Table I. In particular, to test possible improvements of the tagger [23], we need to study the correlation between the signal efficiency ε_S versus the background misidentification

TABLE II.   (Mis)tagging efficiencies for standard and inverted cut order, in the latter case for the $|m_{123} - m_t|$ and dj_{sum} selections. All cuts and tagging parameters are given in Table I. The new HEPTopTagger default setting is indicated.

		Standard	Inverted	
		$|m_{123} - m_t|$	$|m_{123} - m_t|$	dj_{sum}
8 TeV	ε_S	0.331	0.375	0.304
	ε_B	0.014	0.018	0.014
13 TeV	ε_S	0.337	0.394	0.305
	ε_B	0.015	0.021	0.016
		Old default	New default	

probability ε_B. For the standard working point both of these efficiencies are described in Table II. The two-dimensional correlation of ε_S and $1 - \varepsilon_B$ is described by a ROC curve. Any point on this curve corresponds to an optimized parameter setting in the algorithm and can be chosen as the operating point for an analysis. We derive the ROC curves for the HEPTopTagger using a boosted decision tree as implemented in TMVA [34]. In the TMVA analysis we vary the boundaries of the A-shaped constraints $\arctan m_{13}/m_{12}$ and m_{23}/m_{123}. To avoid continuously rerunning the algorithm, we only allow for tighter cuts than the default algorithm. The top mass window which is not part of the actual fat jet algorithm can change without an external constraint, and we include an additional cut on the reconstructed mass ratio $(m_W/m_t)^{\text{rec}}$. For more details on the BDT optimization we refer to Ref. [25].

In the left panel of Fig. 2 we show ROC curves for the reordered HEPTopTagger algorithm for 8 TeV collider energy. We show results for the new standard setup and the high-luminosity setup ordered by the modified Jade distance of Eq. (2). As mentioned before, the efficiency for the signal is defined as the number of tagged tops normalized to the number of hadronically decaying tops with $p_{T,t} >$ 200 GeV and $|\eta_t| < 2.5$. For the background the normalization is given by the number of fat jets fulfilling the same p_T and η criteria. Computed for the full $t\bar{t}$ sample we reach signal efficiencies of 40% for a background rejection over 97.5%. When computed over the entire p_T range of the fat jet or top quark, we see that the algorithm essentially breaks down at signal efficiencies above $\varepsilon_S = 0.6$. The reason is that the number of possibly tagged tops is limited by the number of tops with all three decay subjets inside the fat jet.

For 13 TeV, shown in the right panel of Fig. 2, we break the efficiency into three transverse momentum slices of the top or the fat jets, namely, $p_T = 200$–250 GeV, $p_T = 250$–300 GeV, and $p_T > 300$ GeV. Higher transverse
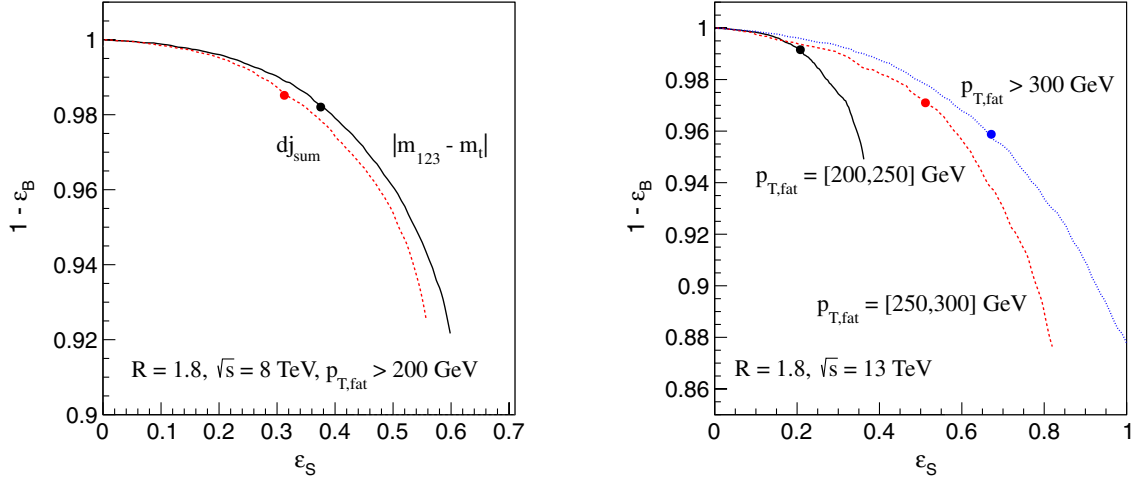
FIG. 2 (color online).   ROC curves for the modified HEPTOPTAGGER on semileptonic $t\bar{t}$ pairs for 8 TeV (left panel) and 13 TeV (right panel) collider energy. The standard working points with the cuts given in Table I are indicated by dots. For 8 TeV we show the new default setup and the high-multiplicity modification. For 13 TeV we quote the performance in slices of $p_{T,\text{fat}}$.

momenta will be statistically limited in the $t\bar{t}$ sample and are not the focus of this study. The signal efficiencies are defined as the number of tags obtained from the considered fat jets divided by the number of hadronically decaying tops in the event sample within the given range of transverse momenta. The combined curve for the $t\bar{t}$ sample will essentially coincide with the lowest p_T bin, simply because of the composition of the signal events. Again, we observe that the signal efficiency is limited in the soft region. Above $p_{T,t} = 300$ GeV we can reach almost 100% signal efficiencies. The performance of the new default working point from Table I is indicated by a dot. Depending on the analysis, we see that over the entire p_T range the HEPTOPTAGGER can reach a QCD background rejection of 99% for signal efficiencies between 20% for soft tops and 40% for hard tops. If required, the optimal working point of the top tagger can be chosen as a function of the fat jet momentum, for example, to guarantee a constant signal efficiency or background rejection according to Fig. 2.

The one remaining question is if the new version of the HEPTOPTAGGER still benefits from the pruned reconstructed top mass [18], as it does for the old version [23]. In terms of the ROC curves shown in Fig. 2 we can compare the new default tagger with the version including the pruned mass. It turns out that the two ROC curves are identical for each transverse momentum slice. The former improvement based on including the pruned mass is already taken into account in the improved efficiencies shown in Table II.

III. ANGULAR CORRELATIONS

To make a conclusive statement about possible improvements to the HEPTOPTAGGER by using angular correlations of the subjets, we need a systematic way to include such angular correlations. Correlations between a pair of subjets

or other objects can be fully described in the basis of spherical harmonics. Fox-Wolfram moments are then constructed as a sum over all $2\ell + 1$ directions, weighted by a free function W_i [24],

$$H_\ell^x = \frac{4\pi}{2\ell + 1} \sum_{m=-\ell}^{\ell} \left| \sum_{i=1}^{N} W_i^x Y_\ell^m(\Omega_i) \right|^2. \quad (3)$$

The index i runs over all N objects. The individual coordinates Ω_i can be replaced by the corresponding angular separation Ω_{ij}, allowing us to write the moments in terms of Legendre polynomials

$$H_\ell^x = \sum_{i,j=1}^{N} W_{ij}^x P_\ell(\cos \Omega_{ij}) \qquad \text{with } W_{ij}^x = W_i^x W_j^x. \quad (4)$$

Two common weights are the transverse momentum or the unit weights [24,25]

$$W_{ij}^T = \frac{p_{Ti} p_{Tj}}{(\sum p_{Ti})^2} \qquad W_{ij}^U = \frac{1}{N^2}. \quad (5)$$

The advantage of the transverse momentum weight is that it suppresses soft and collinear jets, which are hard to correctly describe in QCD. However, tests show us that inside a top tagger the unit weight is more promising. Therefore, we do not use the transverse momentum weight in this analysis. We could in principle also compute these moments over other objects inside the fat jet, for example before filtering or the five subjet structures before reclustering. However, all of this would make our results process dependent and hence not suitable for this study.

Using the unit weight the Fox-Wolfram moments analyze the angular correlations inside the fat jet. We evaluate them in the top rest frame to remove the leading effect from the boost. This means that for the unit weights we do not
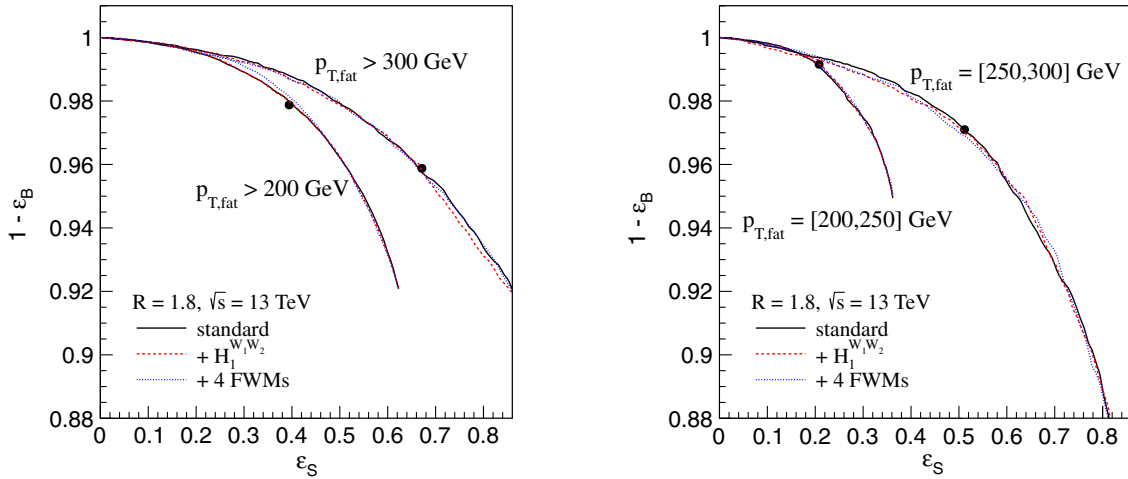
FIG. 3 (color online).   ROC curves for the modified HEPTOPTAGGER including angular correlations via unit-weight Fox-Wolfram moments in slices of $p_{T,\text{fat}}$. The standard working point from Table I is indicated by a dot. We assume a collider energy of 13 TeV.

have to define a reference axis, and only two of the three angles between the subjets are independent. The fourth direction is given by the direction of the fat jet or the boost into the top rest frame.

To quantify the improvement which can be gained from the angular correlation, we evaluate the Fox-Wolfram moments for each combination of subjets using a boosted decision tree as implemented in TMVA. For the angular analysis we label the two subjets which reconstruct m_W best as W_1 and W_2, ordered by transverse momentum. The remaining subjet is then labeled the b jet. As long as we include a full set of correlations in the Fox-Wolfram moments, these names do not matter for the performance. They will only become relevant once we interpret the results. Using TMVA we determine the most decisive moments for each combination of two to four subjets and the boost direction, i.e. two spatial directions out of $\{W_1, W_2, b, \vec{P}_{\text{boost}}\}$. This allows us to define a limited set of Fox-Wolfram moments which we can reliably compare to the purely kinematics-based selection discussed before.

In Fig. 3 we show ROC curves for the full event sample and for slices in the transverse momentum of the fat jet. The purely QCD-inspired selection criteria of Table I are contrasted with the selection including the available angular correlations. The moment with the strongest separation for signal and background is the first moment H_1^U built from the two W decay jets. However, for all four $p_{T,\text{fat}}$ choices we see that including this additional information has no effect on the performance of the tagger.

In addition, we show results including the leading moments from the best sets of momenta. As mentioned above, the leading moment is H_1^U from the (W_1, W_2) selection. Other examples for highly ranked moments are H_2^U from the $(W_1, W_2, \vec{P}_{\text{boost}})$ selection or H_1^U defined over $(W_2, b, \vec{P}_{\text{boost}})$. The results from an optimized tagger

using the best four moments are also shown in Fig. 3, again with no visible improvement.

The bottom line of this systematic analysis of angular correlations in the top tagger is that the angular correlations among the top decay products and the top direction are already included in the QCD-based selection. Apparent improvements are within the reach of the ROC curve. For the given transverse momentum range, adding more angular information does not lead to a measurable improvement of the HEPTOPTAGGER.

IV. N-SUBJETTINESS

A second way to identify boosted hadronically decayed top quarks could be as a combination of a mass-drop criterion with N-subjettiness [35]. This additional observable measures how well a fat jet is described by a given number of subjets. It starts by constructing N reference axes and then measures how well the k fat jet constituents fit to those axes,

$$\tau_N = \frac{\sum_k p_{T,k} \min\left(\Delta R_{1,k}, \Delta R_{2,k}, \ldots, \Delta R_{N,k}\right)}{R_0 \sum_k p_{T,k}}. \quad (6)$$

ΔR is the usual geometric separation and R_0 is an intrinsic cone size, usually the value used to construct the fat jet. Small values of τ_N indicate that the jet is consistent with N or fewer subjets. Consequently, ratios of the kind τ_N/τ_{N-1} allow us to distinguish between jets described by N or $N-1$ substructures. For top tagging the ratio τ_3/τ_2 is expected to be most useful.

Similar to the case of angular correlations studied in the previous section, we combine the HEPTOPTAGGER [7] setup given in Table I with N-subjettiness based on
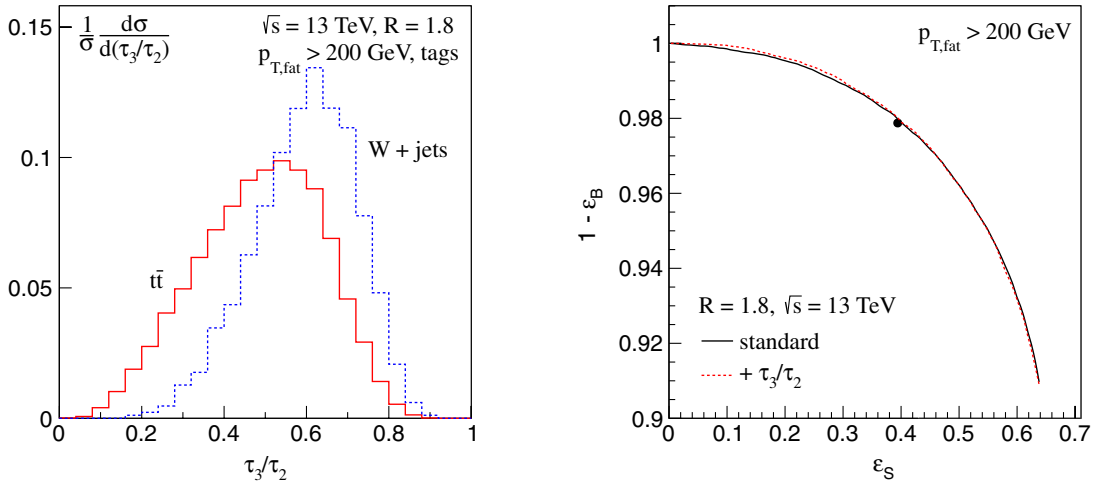
FIG. 4 (color online).   Left panel: τ_3/τ_2 for tagged fat jets. The red solid curves show the $t\bar{t}$ signal, while the blue dotted curves give the $W + $ jets background. Right panel: ROC curves for the combined HEPTOPTAGGER and τ_3/τ_2.

axes using the one-pass-k_T method implemented in SPARTYJET [36].

In the left panel of Fig. 4 we show the τ_3/τ_2 distributions for the fat jets tagged by the new default HEPTOPTAGGER. We see that τ_3/τ_2 without any additional cuts carries information that can be used to distinguish between signal and background. To check the power of this additional variable in addition to the tagging algorithm, we again compute the corresponding ROC curve with a variable combination of tagging parameters and N-subjettiness using boosted decision trees as implemented in TMVA [34]. We show the results in the right panel of Fig. 4: First, we show the new default HEPTOPTAGGER described in Sec. II, allowing for an optimized mass window m_{123} as well as tighter A-shaped mass plane cuts and a cut on m_W/m_t. We then include τ_3/τ_2 in the boosted decision tree and see that it gives a hardly visible improvement in the low efficiency range.

The bottom line of this analysis of a combined mass-drop and N-subjettiness tagger is again that the additional information includes relevant information, but that it does not lead to an improvement compared to an optimized HEPTOPTAGGER setup. The apparent improvement corresponds merely to a shift in the working point of the mass-drop tagger.

V. LOW BOOST

The lesson we learned in Secs. III and IV, namely that adding angular correlations or additional observables to the tagging algorithm has essentially no effect, is limited to sufficiently boosted top quarks for which the algorithm has the chance to identify all three decay jets from mass-drop criteria. In the range of $p_{T,t} = 150$–200 GeV this might not be the case, while the fat jet still includes most of the kinematic information from the top decay. For example, the

softest decay jet might be pushed outside the fat jet and replaced by an initial state QCD jet, but the two leading jets could still be used to identify a massive top decay. For such events the mass-drop criterion will not be efficient enough to separate the signal from the background, which brings us back to angular correlations between the decay products.

One obvious application for a top tagger at low momenta is the associated production of a Higgs with a pair of top quarks [2]. In Table III we show the fraction of events for this process including one or two top quarks with $p_{T,t} > 150$ GeV or $p_{T,t} > 200$ GeV. Reducing the transverse momentum threshold by 50 GeV increases the number of events by 50% for one top tag and by 100% for two top tags.

The default HEPTOPTAGGER has never targeted top quarks with $p_{T,t} < 200$ GeV. This consistency condition is related to the size of the fat jet and based on the assumption that the algorithm has to be able to see all three top decay subjets [7]. In this section we suggest a new analysis step targeting events with $p_{T,t}^{\mathrm{rec}} = 150$–$200$ GeV. In this range we will employ angular correlations through the Fox-Wolfram moments, introduced in the last section.

TABLE III.   Fraction of the total cross section for $t\bar{t}H$ production at 13 TeV, passing a range of cuts on the transverse momentum of the harder top (p_{T,t_1}) or both tops ($p_{T,t}$).

$\sigma_{\mathrm{tot}} = 360$ fb	all $p_{T,H}$	$p_{T,H} > 100$ GeV
all $p_{T,t}$	100%	48%
$p_{T,t_1} > 150$ GeV	59%	37%
$p_{T,t_1} > 200$ GeV	39%	27%
$p_{T,t} > 150$ GeV	29%	16%
$p_{T,t} > 200$ GeV	15%	8.8%

As before, our study is based on semileptonically decaying top pairs. The size of the fat Cambridge-Aachen jet is $R_{\text{fat}} = 1.8$, and it is required to have $p_{T,\text{fat}} > 150$ GeV and $|\eta_{\text{fat}}| < 2.5$. Those fat jets are analyzed with the (new) default HEPTOPTAGGER described in Sec. II. To determine the quality of each top tag with $p_{T,t}^{\text{rec}} = 150$–$200$ GeV we rely on the geometric separation of the parton-level top decay jets and the reconstructed top constituents for a given mapping j_i [23],

$$\Delta R_{\text{sum}}^2 = \sum_{i=1}^{3} \Delta R^2(p_i^{\text{rec}}, p_{j_i}^{\text{parton}}). \qquad (7)$$

We minimize ΔR_{sum}^2 to define the best mapping of parton-level and reconstructed top decay products. Based on the parton-level information we can then assign it to one of three types:

Type 1: All three subjets of the tagged top quark correspond to top decay products at parton level.

Type 2: The two hardest subjets correspond to top decay products; the third subjet does not.

Type 3: This includes everything else.

This way the type-3 category includes events where one or zero subjets correspond to top decay products, but also events where only the hardest subjet cannot be assigned to a top decay parton. In Table IV we see the fraction of type-1 to type-3 tags after requiring a reduced threshold $p_{T,\text{fat}} > 150$ GeV and only considering a low-p_T slice with $p_{T,t}^{\text{rec}} = 150$–$200$ GeV. For the default tagger with these two modifications, 57% of the additional tags are of type-1; i.e. all top decay products can be assigned to parton-level information. For an additional 14% of events the two leading subjets can be linked to top decay product at parton level, while for 29% this matching is problematic.

The critical step at which top decays that are not perfectly matched in the type-2 and type-3 categories fail the default tagging algorithm is the final mass window $m_t^{\text{rec}} = 150$–200 GeV. In the modified low-p_T mode the HEPTOPTAGGER first accepts all tagged tops with

$m_t^{\text{rec}} = 150$–200 GeV, as long as they fulfill the now lower consistency criterion $p_{T,\text{tag}} = 150$–200 GeV.

We then target all events which do not pass the m_t^{rec} condition but fall within the transverse momentum range $p_{T,\text{tag}} = 150$–200 GeV. For these we widen the m_t^{rec} window and add a new requirement for the reconstructed W to top mass ratio. In Table V we quote one working point for illustration purposes. Two cuts on $\arctan(m_{13}/m_{12})$ and m_{23}/m_{123} are part of the A-shaped selection in the original tagging algorithm, which means all events passing the tagging algorithm lie inside this A shape. Just as in the ROC analysis of Sec. II, we now allow for an additional cut on both of these subjet observables. Finally, we include the best Fox-Wolfram moments in the four leading jet selections. The cut values quoted in Table V define one working point on the ROC curve for the low-p_T mode. The corresponding efficiencies for this point are quoted in Table IV. Its efficiency over the $t\bar{t}$ sample with a hadronically decaying top in the same p_T range is significantly increased from 29% to 35%, with a slightly larger fraction of type-2 and type-3 events. In many applications of the top tagger these low-p_T top decays constitute most of the signal sample, as shown for the $t\bar{t}H$ production process in Table III. Here, the low-p_T improvement might increase the overall number of tagged signal events by upto 20%.

To compute a ROC curve for the low-p_T mode, we optimize the tagging parameters only for type-2 tags which did not pass the original algorithm. According to Table IV optimizing on all events would give a significant weight to type-3 events, which would lead to an increased number of tags with very poor top reconstruction. We therefore compute the ROC curve of the low-p_T tagger by optimizing the tagger for type-2 events in the $p_{T,\text{fat}} = 150$–200 GeV band. We then compute the corresponding efficiencies for the entire $t\bar{t}$ sample. In Fig. 5 we compare the performance of the low-p_T mode to the new default tagger shown in Fig. 2. We see, first of all, that the new mode makes the slice with $p_{T,\text{fat}} = 150$–200 GeV competitive with the softest slice in the standard setup. Also, the slice with fat jets within $p_{T,\text{fat}} = 200$–250 GeV benefits from the

TABLE IV. Comparison of tagging results in the new default setup without (left) and with (right) the low-p_T mode. All tags fulfill $p_{T,\text{fat}} > 150$ GeV as well as $p_{T,\text{tag}} = 150$–200 GeV. The working point for the low-p_T mode is given in Table V. The quoted cross section values correspond to the semileptonic $t\bar{t}$ sample.

	Default		Low-p_T mode	
	(mis)tags [fb]	fraction	(mis)tags [fb]	fraction
Type 1	5309	57%	5967	52%
Type 2	1283	14%	1863	16%
Type 3	2712	29%	3601	32%
ε_S	0.287		0.353	
W + jets	1200		1663	
ε_B	0.007		0.010	

TABLE V. Cuts defining the working point used for the low-p_T mode shown in Fig. 4. The values are extracted using simulated annealing.

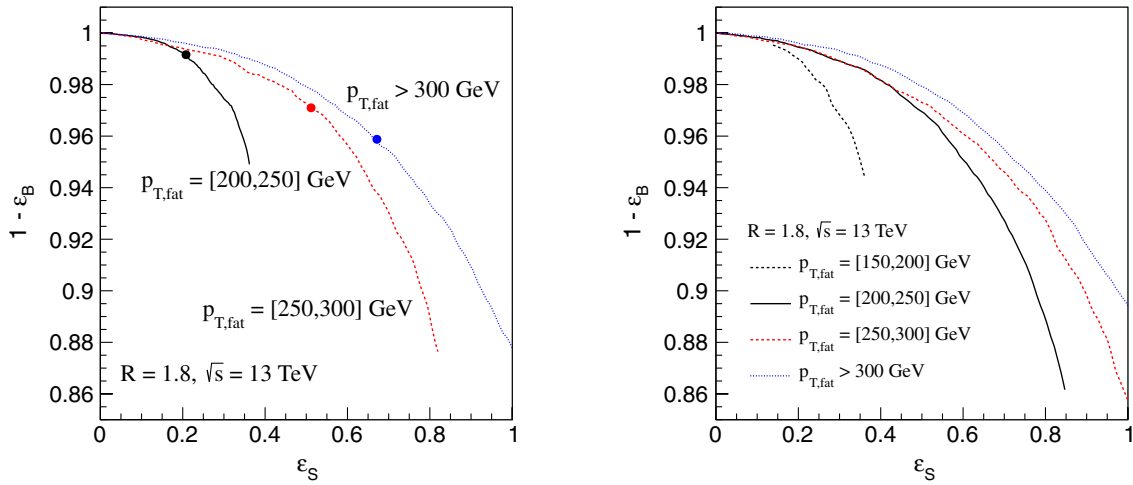|	Min	Max
m_t^{rec} [GeV]	108.	282.
$(m_W/m_t)^{\text{rec}}/(m_W/m_t)$	0.717	1.556
$\arctan(m_{13}/m_{12})$	0.441	0.889
m_{23}/m_{123}	0.412	0.758
$H_1^{W_1 W_2}$	0.048	0.373
$H_2^{p W_1 W_2}$	0.019	0.524
$H_2^{pb W_1 W_2}$	0.044	0.276
$H_1^{pb W_2}$	0.145	0.445

FIG. 5 (color online).   ROC curves for the new standard HEPTOPTAGGER without (left panel) and with (right panel) the new low-p_T mode in slices of $p_{T,\text{fat}}$. The signal performance is given for semileptonic $t\bar{t}$ pairs at 13 TeV collider energy.
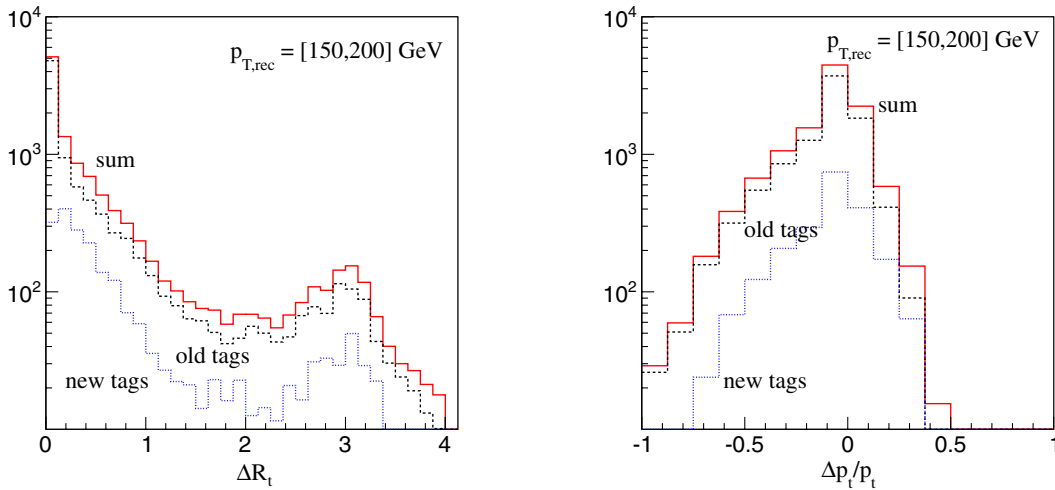

FIG. 6 (color online).   Reconstruction for the original tags (dashed black line), the additional tags in the low-p_T mode (dotted blue line), and all events in the semileptonic $t\bar{t}$ sample (solid red line). We show the angular difference and the relative difference in transverse momentum between the reconstructed top momentum and parton-level truth for all tagged tops.

new mode because a large number of newly tagged events with $p_{T,t}^{\text{rec}} = 150$–$200$ GeV appear in that slice. As mentioned above, in the new version the cuts and tagging criteria can be optimized depending on the transverse momentum, for example, of the fat jet, to improve a given analysis.

Before we can make use of the significant improvement documented above, we need to ensure that for the tops tagged in the low-p_T mode, the HEPTOPTAGGER reconstructs the direction and the 4-momentum as well as for the original setup. In Fig. 6 we see that the dedicated low-p_T tags inside the HEPTOPTAGGER have almost the same quality of the standard tags in the same transverse momentum range [23]. We show the geometric distance ΔR_t between the reconstructed top momentum and the parton-level top momentum as well as the normalized

deviation in transverse momentum, $\Delta p_t/p_t = (p_{T,t}^{\text{rec}} - p_{T,t}^{\text{true}})/p_{T,t}^{\text{rec}}$. The only slight weakness of the low-p_T mode is the depleted region with excellent angular resolution, i.e. $\Delta R_t \lesssim 0.1 \ll R_{\text{fat}} = 1.8$. We actually expect that this precision can be improved by a dedicated calibration procedure, which is beyond the capabilities of the kind of study we present here.

VI. OUTLOOK

In this top tagging study we defined the new default setup of the HEPTOPTAGGER for the upcoming 13 TeV run, with a focus on moderate boosts of $p_{T,t} > 150$ GeV. The entire study is based on the experimentally accessible semileptonic $t\bar{t}$ sample. Our key results are as follows.

(1) For large fat jets with $R_{\text{fat}} = 1.8$ we define a new default setup with reduced shaping of the multijet

background. In addition, we provide a specific high-multiplicity mode for the tagger.

(2) We give ROC curves which allow us to define the most appropriate working points depending on the transverse momentum of the fat jet. An optimal working point can be chosen for individual analyses, including p_T-dependent parameter choices.

(3) Including angular correlations after the QCD-inspired selection does not improve the tagging performance for $p_{T,\text{fat}} > 200$ GeV. The same is true for the pruned mass as an additional observable. The QCD-inspired tagging algorithm appears to be highly efficient in extracting the available information.

(4) Similarly, combining the HEPTopTagger with N-subjettiness does not give significant improvement in terms of the ROC curve.

(5) We define a low-p_T mode probing tops down to $p_{T,t} = 150$ GeV, which makes use of angular correlations for tops with only part of their decay products captured inside the fat jet. For the $t\bar{t}$ sample this leads to a signal efficiency of 35% in the targeted momentum range.

With those modifications we expect the HEPTopTagger to be even more useful for a wide range of analyses to come, including $t\bar{t}H$ searches.

ACKNOWLEDGMENTS

[1] D. E. Morrissey, T. Plehn, and T. M. P. Tait, Phys. Rep. **515**, 1 (2012).

[2] T. Plehn, G. P. Salam, and M. Spannowsky, Phys. Rev. Lett. **104**, 111801 (2010).

[3] For a nice description of the experimental challenges see J. Cammin and M. Schumacher, Report No. ATL-PHYS-2003-024.

[4] See e.g. T. Plehn and M. Rauch, Europhys. Lett. **100**, 11002 (2012).

[5] See e.g. D. Lopez-Val, T. Plehn, and M. Rauch, J. High Energy Phys. 10 (2013) 134.

[6] P. Meade and M. Reece, Phys. Rev. D **74**, 015010 (2006); J. Ellis, F. Moortgat, G. Moortgat-Pick, J. M. Smillie, and J. Tattersall, Eur. Phys. J. C **60**, 633 (2009); K. Rolbiecki, J. Tattersall, and G. Moortgat-Pick, Eur. Phys. J. C **71**, 1517 (2011); M. Perelstein and A. Weiler, J. High Energy Phys. 03 (2009) 141.

[7] T. Plehn, M. Spannowsky, M. Takeuchi, and D. Zerwas, J. High Energy Phys. 10 (2010) 078; http://www.thphys .uni-heidelberg.de/~plehn/.

[8] K. Rehermann and B. Tweedie, J. High Energy Phys. 03 (2011) 059; T. Plehn, M. Spannowsky, and M. Takeuchi, J. High Energy Phys. 05 (2011) 135.

[9] W. Skiba and D. Tucker-Smith, Phys. Rev. D **75**, 115010 (2007); B. Holdom, J. High Energy Phys. 03 (2007) 063; M. Gerbush, T. J. Khoo, D. J. Phalen, A. Pierce, and D. Tucker-Smith, Phys. Rev. D **77**, 095003 (2008); G. Brooijmans, Reports No. ATL-PHYS-CONF-2008-008 and No. ATL-COM-PHYS-2008-001 (2008).

[10] See e.g. K. Agashe, A. Belyaev, T. Krupovnickas, G. Perez, and J. Virzi, Phys. Rev. D **77**, 015003 (2008); V. Barger, T. Han, and D. G. E. Walker, Phys. Rev. Lett. **100**, 031801 (2008); B. Lillie, L. Randall, and L.-T. Wang, J. High Energy Phys. 09 (2007) 074; U. Baur and L. H. Orr, Phys. Rev. D **77**, 114001 (2008); P. Fileviez Perez, R. Gavin, T. McElmurry, and F. Petriello, Phys. Rev. D **78**, 115017

(2008). U. Baur and L. H. Orr, Phys. Rev. D **76**, 094012 (2007).

[11] F. Kling, T. Plehn, and M. Takeuchi, Phys. Rev. D **86**, 094029 (2012).

[12] M. R. Buckley, T. Plehn, and M. Takeuchi, J. High Energy Phys. 08 (2013) 086; M. R. Buckley, T. Plehn, T. Schell, and M. Takeuchi, J. High Energy Phys. 02 (2014) 130.

[13] A. Abdesselam et al., Eur. Phys. J. C **71**, 1661 (2011); T. Plehn and M. Spannowsky, J. Phys. G **39**, 083001 (2012); A. Altheimer et al., arXiv:1311.2708.

[14] M. H. Seymour, Z. Phys. C **62**, 127 (1994); J. M. Butterworth, B. E. Cox, and J. R. Forshaw, Phys. Rev. D **65**, 096014 (2002).

[15] J. M. Butterworth, A. R. Davison, M. Rubin, and G. P. Salam, Phys. Rev. Lett. **100**, 242001 (2008).

[16] D. E. Kaplan, K. Rehermann, M. D. Schwartz, and B. Tweedie, Phys. Rev. Lett. **101**, 142001 (2008).

[17] L. G. Almeida, S. J. Lee, G. Perez, I. Sung, and J. Virzi, Phys. Rev. D **79**, 074012 (2009); L. G. Almeida, S. J. Lee, G. Perez, G. F. Sterman, I. Sung, and J. Virzi, Phys. Rev. D **79**, 074017 (2009); L. G. Almeida, S. J. Lee, G. Perez, G. Sterman, and I. Sung, Phys. Rev. D **82**, 054034 (2010).

[18] S. D. Ellis, C. K. Vermilion, and J. R. Walsh, Phys. Rev. D **80**, 051501 (2009); **81**, 094023 (2010); C. K. Vermilion, arXiv:1101.1335.

[19] J. Thaler and L.-T. Wang, J. High Energy Phys. 07 (2008) 092; D. Krohn, J. Thaler, and L.-T. Wang, J. High Energy Phys. 06 (2009) 059; 02 (2010) 084.

[20] J. Thaler and K. Van Tilburg, J. High Energy Phys. 03 (2011) 015; 02 (2012) 093.

[21] A. Hook, M. Jankowiak, and J. G. Wacker, J. High Energy Phys. 04 (2012) 007; M. Jankowiak and A. J. Larkoski, J. High Energy Phys. 06 (2011) 057; M. Jankowiak and A. J. Larkoski, J. High Energy Phys. 04 (2012) 039; D. E. Soper and M. Spannowsky, Phys. Rev. D **87**, 054012

(2013); S. Schätzel and M. Spannowsky, Phys. Rev. D **89**, 014007 (2014).

[22] ATLAS Collaboration, J. High Energy Phys. 01 (2013) 116; ATLAS Collaboration, Report No. ATLAS-CONF-2013-084; G Piacquadio, Report No. CERN-THESIS-2010-027; G Kasieczka, Ph.D. thesis, http://www.ub.uni-heidelberg.de/archiv/14941.

[23] T. Plehn, M. Spannowsky, and M. Takeuchi, Phys. Rev. D **85**, 034029 (2012).

[24] G. C. Fox and S. Wolfram, Phys. Rev. Lett. **41**, 1581 (1978); R. D. Field, Y. Kanev, and M. Tayebnejad, Phys. Rev. D **55**, 5685 (1997).

[25] C. Bernaciak, M. S. A. Buschmann, A. Butter, and T. Plehn, Phys. Rev. D **87**, 073014 (2013); C. Bernaciak, B. Mellado, T. Plehn, X. Ruan, and P. Schichtel, Phys. Rev. D **89**, 053006 (2014).

[26] T. Plehn, P. Schichtel, and D. Wiegand, Phys. Rev. D **89**, 054002 (2014).

[27] M. L. Mangano, M. Moretti, F. Piccinini, R. Pittau, and A. D. Polosa, J. High Energy Phys. 07 (2003) 001.

[28] T. Sjostrand, S. Mrenna, and P. Z. Skands, J. High Energy Phys. 05 (2006) 026.

[29] M. L. Mangano, M. Moretti, and R. Pittau, Nucl. Phys. **B632**, 343 (2002).

[30] Y. L. Dokshitzer, G. D. Leder, S. Moretti, and B. R. Webber, J. High Energy Phys. 08 (1997) 001; M. Wobisch and T. Wengler, arXiv:hep-ph/9907280.

[31] M. Cacciari and G. P. Salam, Phys. Lett. B **641**, 57 (2006); M. Cacciari, G. P. Salam, and G. Soyez, Eur. Phys. J. C **72**, 1896 (2012); http://fastjet.fr.

[32] ATLAS Collaboration, J. High Energy Phys. 09 (2013) 076.

[33] W. Bartel *et al.* (JADE Collaboration), Z. Phys. C **33**, 23 (1986).

[34] A. Höcker *et al.*, *Proc. Sci.*, ACAT2007 (**2007**) 040 [arXiv:physics/0703039]; P. Speckmayer, A. Höcker, J. Stelzer, and H. Voss, J. Phys. Conf. Ser. **219**, 032057 (2010); http://tmva.sourceforge.net.

[35] J. Thaler and K. Van Tilburg, J. High Energy Phys. 03 (2011) 015; 02 (2012) 093; I. W. Stewart, F. J. Tackmann, and W. J. Waalewijn, Phys. Rev. Lett. **105**, 092002 (2010).

[36] P.-A. Delsart, K. L. Geerlings, J. Huston, B. T. Martin, and C. K. Vermilion, arXiv:1201.3617.